

# Extended Metal-Insulator Crossover with Strong Antiferromagnetic Spin Correlation in Half-Filled 3D Hubbard Model

Yu-Feng Song,<sup>1,2</sup> Youjin Deng,<sup>1,3,\*</sup> and Yuan-Yao He<sup>2,4,3,†</sup>

<sup>1</sup>Hefei National Laboratory for Physical Sciences at Microscale and Department of Modern Physics, University of Science and Technology of China, Hefei, Anhui 230026, China

<sup>2</sup>Institute of Modern Physics, Northwest University, Xi'an 710127, China

<sup>3</sup>Hefei National Laboratory, University of Science and Technology of China, Hefei 230088, China

<sup>4</sup>Shaanxi Key Laboratory for Theoretical Physics Frontiers, Xi'an 710127, China

(Dated: April 16, 2024)

The Hubbard model at temperature above the Néel transition, despite of being a paramagnet, can exhibit rich physics due to the interplay of Fermi surface, on-site interaction  $U$  and thermal fluctuations. Nevertheless, the understanding of the crossover physics remains only at a qualitative level, because of the intrinsically smooth behavior. Employing an improved variant of the *numerically exact* auxiliary-field quantum Monte Carlo algorithm equipped with numerical analytic continuation, we obtain a broad variety of static and dynamical properties of the three-dimensional Hubbard model at half filling, quantitatively determine the crossover boundaries, and observe that the metal-insulator crossover state, in which antiferromagnetic spin correlations appear strongest, exists over an extended regime in between the metallic state for small  $U$  and the Mott insulator for large  $U$ . In particular, the Widom line, corresponding to the most rapid suppression of double occupancy as  $U$  increases, is found to fully reside in the metallic Fermi liquid regime, in contrast to the conventional intuition that it is a representative feature for entering the Mott insulator. Beside providing a reliable methodology for numerical study of crossover physics, our work can also serve as a timely and important guideline for the most recent optical lattice experiments.

The Mott metal-insulator transition (MIT) [1, 2] has been a long-standing topic since the early days of condensed matter physics. It has been experimentally observed in variously realistic materials, ranging from the typical representative of transition metal oxides [3–6] to the latest hotspot of twisted 2D moiré systems [7–9]. While the Mott transition is mostly found to be first order [4, 10, 11], recent studies show that it can also be continuous [12–14]. The modern view of this phenomenon follows the original ideas of Mott [15, 16] and Hubbard [17] that the Coulomb interaction between electrons plays a central role as splitting the conduction band and thus opening a charge gap. However, the complete understanding and characterization of Mott transition still remain as a big challenge, especially in the aspect of connecting the experimental observations with Hubbard models [18–20].

A great achievement for this problem came from the insight of dynamical mean-field theory (DMFT) calculations in 1990s [2, 10]. In infinite dimensions ( $d \rightarrow \infty$ ) where the method becomes exact, the first-order MIT with a critical end point at finite temperature was successfully recovered in single-band repulsive Hubbard model [21–24]. Since then, DMFT has served as the leading method and sometimes the only available technique to study the Mott MIT transitions in various Hubbard models [11, 25–28]. However, turning to the physically relevant two and three dimensions, whether the Mott transition exists in the paramagnetic (PM) phase of Hubbard model is still controversial due to the uncontrolled approximation in DMFT calculations and the competition of possible magnetic ordering in the model. Inherited

from the  $d \rightarrow \infty$  limit, DMFT still obtains first-order Mott transition for lower dimensional Hubbard models [29–35] even at half filling without frustration [30, 32] for which the system hosts the long-range antiferromagnetic (AFM) order for arbitrary on-site repulsion in the ground state. Thus, more accurate and even unbiased simulation of Hubbard model is crucial for studying the Mott physics and clarifying the above problem.

One closely related example is the recent study of two-dimensional (2D) repulsive Hubbard model at half filling on square lattice with diagrammatic quantum Monte Carlo (QMC) method [36, 37], which precludes the existence of Mott transition. Instead, a crossover from Fermi liquid to insulating behavior at finite temperatures was identified from the results of self-energy [36], spin and charge correlations [37]. Comparing to the 2D case, the three-dimensional (3D) Hubbard model at half filling can develop a low-temperature AFM ordered phase for all interaction strengths [38–42], which also prohibits the Mott transition at low temperatures. Besides, the metallic and Mott insulating states still exist approaching the weak and strong interaction limits, and their connection in the interaction strength axis remains unexplored in 3D case. As a result, a careful study for the metal-to-insulator process with its thorough characterization in the normal phase of 3D half-filled Hubbard model is demanded to unveil the correlation-driven mechanism.

In this work, we address the above issues by systematically exploring the Mott physics above the AFM Néel transition in half-filled 3D Hubbard model with auxiliary-field quantum Monte Carlo (AFQMC) method. In a numerically unbiased manner, we provide a multimessen-

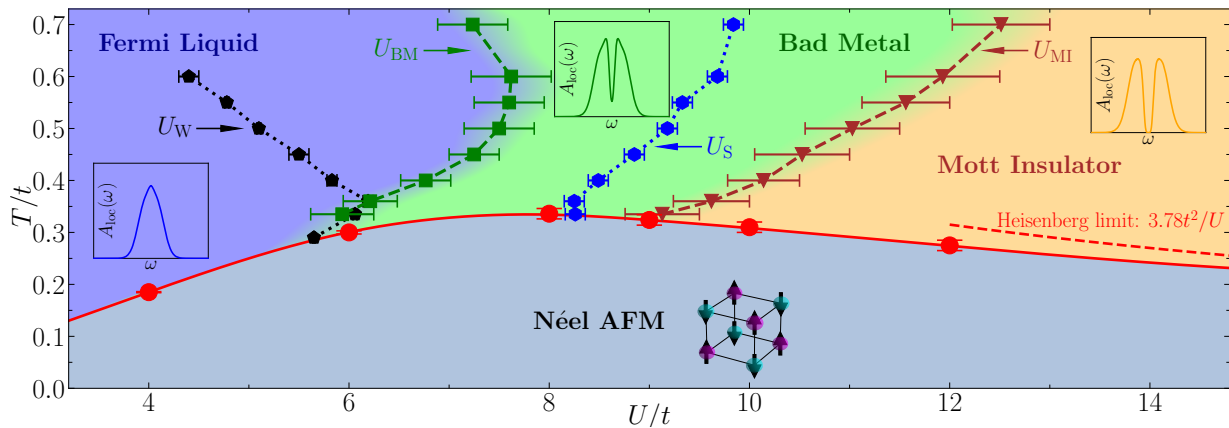


FIG. 1. Phase diagram of half-filled 3D Hubbard model from our AFQMC calculations. Red circles show Néel transition temperatures  $T_N$ , and the solid red line connecting them is a interpolation encoding the result of Heisenberg limit [43]  $T_N = 3.78t^2/U$  (dashed red line). Above  $T_N$ , Fermi Liquid and Mott Insulator exist in the weakly and strongly interacting regimes respectively, and in between the Bad Metal emerges as the metal-insulator crossover. The onsets of Bad Metal and Mott Insulator as  $U_{BM}$  and  $U_{MI}$  are shown by green squares and brown triangles. Crossing  $U_{BM}$  and  $U_{MI}$ , the smooth crossover without any singularity is observed in all physical observables. The peak locations of AFM structure factor (as  $U_S$ ) are plotted as blue hexagons, which reside almost in the center of Bad Metal indicating strong AFM spin correlation. The black pentagons represents the “Widom line” (as  $U_W$ ) as the peak location of  $-\partial D/\partial U$  with  $D$  as the double occupancy.

ger study for the evolution of the system along with increasing interaction strength, incorporating the results of single-particle spectral function, quasiparticle weight, spin correlations, entropy and double occupancy. We elucidate that, instead of the celebrated Mott transition, an extended metal-insulator crossover displaying strong AFM spin correlation emerges. Moreover, we find that the double occupancy fails to characterize this crossover.

We study the half-filled 3D Hubbard model on simple cubic lattice with the Hamiltonian as

$$\hat{H} = -t \sum_{\langle ij \rangle \sigma} (c_{i\sigma}^\dagger c_{j\sigma} + h.c.) + U \sum_{\mathbf{i}} \left( \hat{n}_{i\uparrow} \hat{n}_{i\downarrow} - \frac{\hat{n}_{i\uparrow} + \hat{n}_{i\downarrow}}{2} \right),$$

where  $\hat{n}_{i\sigma} = c_{i\sigma}^\dagger c_{i\sigma}$  is the density operator with  $\sigma$  ( $=\uparrow$  or  $\downarrow$ ) denoting spin. We set the nearest-neighbor (NN) hopping  $t$  as the energy unit, and focus on repulsive interaction  $U > 0$ . This model has Néel AFM ordered ground state [38], and at finite temperature it exhibits continuous AFM-PM phase transition which belongs to the 3D Heisenberg universality class [44]. We then apply the finite-temperature AFQMC algorithm [45–50] encoding the most recent developments [51] to study the interaction-driven Mott physics in this model, which is sign problem free due to the particle-hole symmetry. We perform numerical simulations for periodic supercells with  $N_s = L^3$  (and  $L$  as the linear system size) lattice sites. Our calculations reach  $L = 20$  for static observables and  $L = 12$  for dynamic properties [51].

We first focus on the phase diagram of half-filled 3D Hubbard model from our AFQMC simulations as presented in Fig. 1. The highest temperature in our sim-

ulations is  $T/t = 0.7$ , much lower than the Fermi temperature  $T_F/t = 6$  of the system. As mentioned above, the Néel AFM phase occupies the low temperature region for all interactions. With significant improvements in the precision control and dealing with the finite-size effect in AFQMC calculations, we obtain the most accurate results of the Néel transition temperatures to date for representative interaction strengths [51], via the standard finite-size scaling of AFM structure factor results up to  $L = 20$  using the known critical exponents. Our results illustrate the highest transition temperature  $T_N \sim 0.33t$  achieved around  $U = 8t$ . These are quantitatively comparable to the results in previously unbiased calculations [39, 41].

The contents in the normal phase above the Néel transition in the phase diagram summarize our main results in this work. In the weakly interacting regime, the correlated Fermi Liquid state appears as an adiabatical evolution from  $U = 0$  case, and its fingerprint signature is the coherence peak in local single-particle spectral function  $A_{loc}(\omega)$  at Fermi energy. Approaching the strong interaction limit, the system should be a Mott Insulator exhibiting a fermionic gap as  $A_{loc}(\omega \sim 0) = 0$ , which survives as long as the temperature energy scale  $\sim k_B T$  is smaller than the  $T = 0$  gap of the system. Between these two limits, our numerical results clearly reveal an intermediate regime for which the spectra  $A_{loc}(\omega)$  shows a dip around Fermi energy. We adopt the term Bad Metal [52] for this metal-insulator crossover regime. With increasing  $U/t$ , our results of physical observables only show smooth crossover without any singularity, suggesting the absence of phase transition. The three regimes with their  $A_{loc}(\omega)$  features (as insets) and the boundaries defined

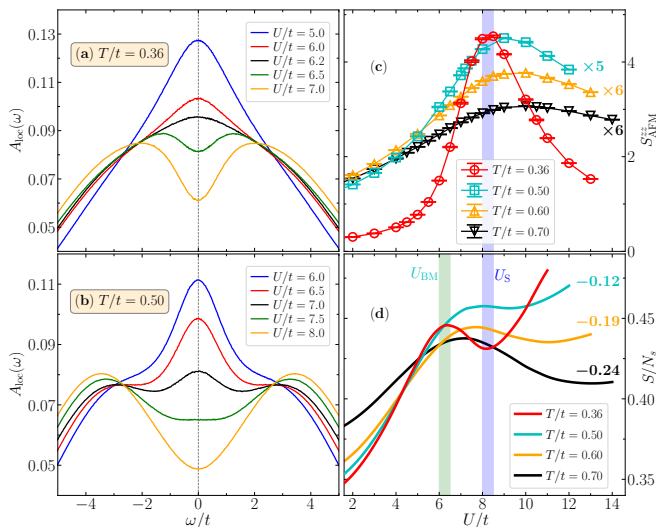


FIG. 2. Local single-particle spectral function  $A_{\text{loc}}(\omega)$  crossing the onset of bad metal ( $U_{\text{BM}}$ ) for (a)  $T/t = 0.36$  and (b)  $T/t = 0.50$ . Panel (c) and (d) plots thermal entropy per site  $S/N_s$  and AFM structure factor  $S_{\text{AFM}}^{zz}$  for four temperatures, respectively. For  $T/t = 0.50, 0.60, 0.70$ , the  $S/N_s$  results are shifted by  $-0.12, -0.19, -0.24$ , and  $S_{\text{AFM}}^{zz}$  data are scaled by a factor  $\times 5, \times 6, \times 6$ , to fit into the plots. The uncertainty of  $S/N_s$  is indicated by the thickness of the lines. For  $T/t = 0.36$ , the result of  $U_{\text{BM}}$  determined from  $A_{\text{loc}}(\omega)$  in (a) as the green shading and the peak location range of  $S_{\text{AFM}}^{zz}$  as the blue shading are shown in (b) and (c).

as the onsets of Bad Metal (as  $U_{\text{BM}}$ ) and Mott Insulator (as  $U_{\text{MI}}$ ) from our simulations are shown in Fig. 1. Additional results of peak locations of AFM structure factor as  $U_{\text{S}}$  and the Widom line as  $U_{\text{W}}$  versus  $U/t$  are also included in the plot. The former resides in the center of Bad Metal regime meaning that this crossover region has strong AFM spin correlation. The latter steps into the Fermi Liquid regime indicating that the double occupancy has little connection with the metal-insulator crossover in this system at  $T/t \geq 0.35$ . In the following, we present detailed results related to the phase diagram.

We first probe the onset of Bad Metal  $U_{\text{BM}}$  via the local spectral function  $A_{\text{loc}}(\omega)$ , which is obtained from the dynamic single-particle Green's function  $G_{\text{loc}}(\tau) = (2N_s)^{-1} \sum_{i\sigma} \langle c_{i\sigma}(\tau) c_{i\sigma}^\dagger \rangle$  using the stochastic analytic continuation (SAC) method [53, 54]. The  $A_{\text{loc}}(\omega)$  results for  $T/t = 0.36$  and  $T/t = 0.50$  are plotted in Fig. 2(a) and (b) [Note that  $A_{\text{loc}}(\omega)$  is symmetric about  $\omega = 0$  at half filling]. For increasing  $U/t$ , we see that  $A_{\text{loc}}(\omega)$  around  $\omega = 0$  is gradually suppressed and it smoothly evolves from the coherence peak structure to the shape of two broaden peaks at finite  $\omega$  indicating the formation of upper and lower Hubbard bands. This dip signature emerges due to the lack of low-energy fermionic excitations, and thus marks the entrance into the Bad Metal regime. We determine  $U_{\text{BM}}$  as the interaction strength where the coherence peak of  $A_{\text{loc}}(\omega)$  at  $\omega = 0$  disap-

pears. Its error bar is estimated. We further obtain  $U_{\text{drop}}$  where  $A_{\text{loc}}(\omega = 0)$  drops by 10% of the value at the left or right fringe, and then take  $(U_{\text{drop}} - U_{\text{BM}})$  as the error bar of  $U_{\text{BM}}$  to include the possible uncertainty in SAC calculations. Such procedure acquires the results  $U_{\text{BM}} = 6.21(27)$  for  $T/t = 0.36$  and  $U_{\text{BM}} = 7.11(29)$  for  $T/t = 0.50$ .

Besides the dip of  $A_{\text{loc}}(\omega)$ , the system also shows intriguing behaviors regarding the spin fluctuation when crossing  $U_{\text{BM}}$  and entering the Bad Metal regime. We quantify this property via the AFM structure factor defined as  $S_{\text{AFM}}^{zz} = N_s^{-1} \sum_{ij} (-1)^{i+j} \langle \hat{s}_i^z \hat{s}_j^z \rangle$ , and present its results versus  $U/t$  for fixed temperatures in Fig. 2(c). We observe that  $S_{\text{AFM}}^{zz}$  increases rapidly around  $U_{\text{BM}}$ , reach the maximum, and then drops towards the strong interaction limit. The peak and the successive decrease of  $S_{\text{AFM}}^{zz}$  with increasing  $U/t$  can be understood from the reducing coupling constant  $J = 4t^2/U$  of the effective Heisenberg model description of the Hubbard model. We obtain the peak location of  $S_{\text{AFM}}^{zz}$  as  $U_{\text{S}}$ , and see that it almost follows the center of the Bad Metal regime as shown in Fig. 1. Similar results can be obtained for the NN spin-spin correlation and spin correlation length with comparable values of  $U_{\text{S}}$  [51]. These together manifest the strong AFM spin correlation as an alternative characterization of the Bad Metal in the normal phase.

We further find that the thermal entropy  $S$  can reproduce the above results of  $U_{\text{BM}}$ , and it can serve as a bridge to connect the behaviors of  $A_{\text{loc}}(\omega)$  and  $S_{\text{AFM}}^{zz}$  in the crossover regime. Here we have developed a fully new scheme to calculate  $S$  along the  $U/t$  axis for fixed temperature via the double occupancy [51]. In Fig. 2(d), we show the entropy per site  $S/N_s$  for the same fixed temperatures as Fig. 2(c). With increasing  $U/t$ , the entropy first increases and reaches a maximum. We verify that the peak location is well consistent with  $U_{\text{BM}}$  for all the temperatures. This reason for this coincidence is that, in correlated Fermi liquid, the entropy is proportional to the effective mass of fermions which generally grows with increasing interaction. Thus, the peak of entropy can be taken as the termination of the Fermi Liquid regime and the entrance into the crossover. For  $U > U_{\text{BM}}$ , the entropy decreases and develops local minimum. We find that the location of this minimum is well consistent with  $U_{\text{S}}$  (peak location of  $S_{\text{AFM}}^{zz}$ ) for  $T/t \leq 0.50$  while it is larger than  $U_{\text{S}}$  for higher temperatures. This could be explained by decomposing contributions to the entropy into charge and spin channels, i.e.,  $S = S_c + S_s$ . For charge channel,  $S_c$  should track the result of  $A_{\text{loc}}(\omega = 0)$ , while  $S_s$  from spin channel behaves oppositely with  $S_{\text{AFM}}^{zz}$ . Thus, once entering Bad Metal regime,  $S_c$  should monotonically decrease while  $S_s$  first decreases to a local minimum and then increases again and finally saturates to  $\ln 2$  reaching  $U = \infty$  limit. This also highlights the peak location of entropy as the onset of Bad Metal regime. Moreover, for  $T/t \leq 0.50$ ,

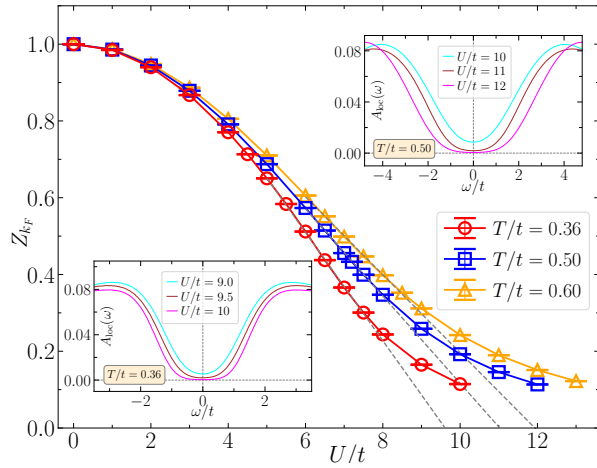


FIG. 3. Determination of the onset of Mott insulator ( $U_{\text{MI}}$ ). The main plot shows the quasiparticle weight  $Z_{k_F}$  versus  $U/t$  for  $T/t = 0.36, 0.50, 0.60$ . Linear fittings (gray dashed lines) are performed for the QMC data in the middle range, and the intercepts of  $U/t$  corresponding to extrapolated  $Z_{k_F} = 0$  are taken as the center values of  $U_{\text{MI}}$ . The local single-particle spectral function  $A_{\text{loc}}(\omega)$  for  $T/t = 0.36$  and  $0.50$  plotted in the insets confirm that  $U_{\text{MI}}$  obtained from  $Z_{k_F}$  indeed corresponds to the entrance into Mott insulator with  $A_{\text{loc}}(\omega = 0) \sim 0$ .

$A_{\text{loc}}(\omega = 0)$  at  $U = U_S$  is pretty small, indicating vanishing  $S_c$ . As a result, the local minimum of the entropy is dominated by  $S_s$ , and thus its location conforms with  $U_S$ . However, for higher temperatures, the contribution of  $S_c$  becomes more significant due to more charge excitations. This together with the valley structure of  $S_s$  shift the local minimum of total entropy to a larger value of  $U$  comparing to  $U_S$ , as the results shown in Fig. 2(d) for  $T/t = 0.60$  and  $0.70$ .

We then turn to onset of Mott Insulator  $U_{\text{MI}}$  in the phase diagram. To avoid the ambiguity of  $A_{\text{loc}}(\omega = 0) = 0$ , we first determine  $U_{\text{MI}}$  from the quasiparticle weight at the Fermi surface as  $Z \approx [1 - \text{Im}\Sigma_\sigma(\mathbf{k}_F, i\omega_0)/\omega_0]^{-1}$ , and then take the results of  $A_{\text{loc}}(\omega = 0)$  as supplementary tool to estimate the uncertainty. And we compute the self energy  $\Sigma_\sigma(\mathbf{k}_F, i\omega_0)$  with  $\mathbf{k}_F$  as Fermi wave vector and  $\omega_0 = \pi/\beta$  via the Dyson Equation. We have performed additional average of  $Z$  results at all  $\mathbf{k}_F$  points since we find that the half-filled 3D Hubbard model is highly isotropic at the Fermi surface for various properties. The number  $(1 - Z)$  measures the interaction induced transfer of spectral weight around  $\omega = 0$  to the incoherent Hubbard bands. Thus the exact  $Z = 0$ , which only exist at  $T = 0$  for finite  $U$ , marks the Mott insulator phase. The results of  $Z$  versus  $U/t$  for  $T/t = 0.36, 0.50$  and  $0.60$  are shown the main plot of Fig. 3. With increasing  $U/t$ , the quantity decreases from unity in the noninteracting limit to a small residual value rounded off by the finite temperature. We take  $U_{\text{MI}}$  as the interaction strength where a linear extrapolation of  $Z$  with

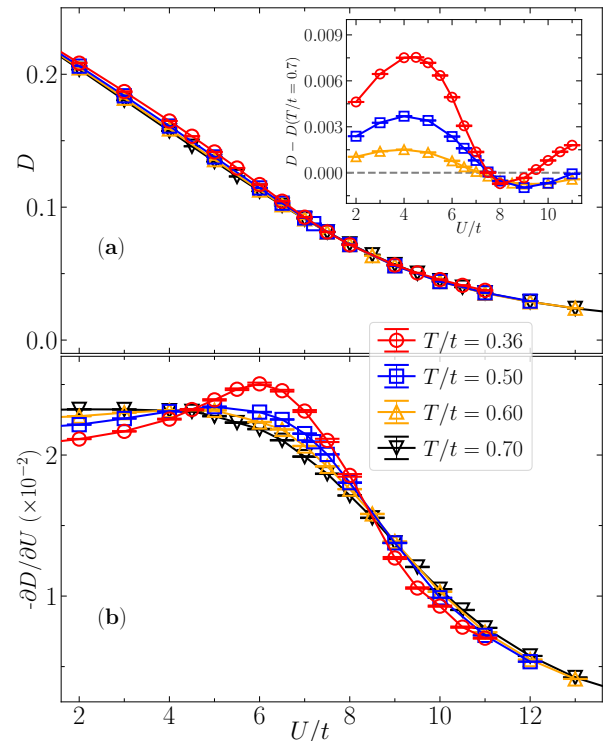


FIG. 4. Double occupancy  $D$  and its first-order derivative  $-\partial D/\partial U$  versus  $U/t$  for four temperatures. The inset in (a) shows the relative  $D$  differences with that of  $T/t = 0.70$ . In (b), the peak location of  $-\partial D/\partial U$  is taken as  $U_W$  of the Widom line for  $T/t = 0.36, 0.50$  and  $0.60$ , while there is no peak for  $T/t = 0.70$ . Note that the  $-\partial D/\partial U$  results in (b) are directly computed from AFQMC simulations instead of the numerical derivative.

intermediate  $U/t$  reaches zero [25, 51]. We then obtain the interaction strength  $U_A$  where the spectra satisfies  $A_{\text{loc}}(\omega = 0) \leq 0.002$ , and take  $|U_A - U_{\text{MI}}|$  as the uncertainty of  $U_{\text{MI}}$ . The corresponding results of  $A_{\text{loc}}(\omega)$  around  $U_{\text{MI}}$  are shown in insets of Fig. 3. This generates  $U_{\text{MI}} = 9.62(38)$  for  $T/t = 0.36$  and  $U_{\text{MI}} = 11.03(47)$  for  $T/t = 0.50$ . Combining all the results, the full curve of  $U_{\text{MI}}$  in Fig. 1 takes almost linear relation with temperature as  $U_{\text{MI}} \propto T$ . This demonstrate the nature of the finite-temperature Mott Insulator: the  $T = 0$  gap of the system which is proportional to  $U$  overtakes the temperature energy scale in the strongly interacting regime.

The double occupancy  $D = N_s^{-1} \sum_i \langle \hat{n}_{i\uparrow} \hat{n}_{i\downarrow} \rangle$  is usually applied as a tool to detect the Mott transition [24–28, 55] in Hubbard models, based on its relation with total energy  $E_g$  as  $D = \partial E_g/\partial U$  at  $T = 0$  and with the free energy  $F$  as  $D = \partial F/\partial U$  at finite temperature [51]. It typically exhibits discontinuity and inflection point around the first-order and continuous Mott transition, respectively. In the system we study, the Mott transition is replaced by the metal-insulator crossover, and thus it represents a fully new situation. We present the numerical results of  $D$  and  $\partial D/\partial U$  versus  $U/t$  for

fixed temperatures in Fig. 4. Note that we have developed a new method to directly compute the derivative  $\partial D/\partial U$  in AFQMC simulations [51], which avoids the numerical differentiation. We see that the double occupancy simply decreases with increasing  $U/t$ , and its temperature variation is quite small for  $0.36 \leq T/t \leq 0.70$  (see inset of Fig. 4(a) as the differences of  $D$  relative to  $T/t = 0.70$ ). Moreover, for  $T/t \leq 0.60$ , the curve of  $D$  has inflection point as signified by the broad peak of  $\partial D/\partial U$  results in Fig. 4(b), while such behaviors disappear for  $T/t \geq 0.70$ . Collecting the peak locations of  $\partial D/\partial U$  for different temperatures forms the Widom line as the  $U_W$  curve in Fig. 1, which fully resides in the Fermi liquid regime and even moves towards smaller  $U$  for  $T/t \geq 0.36$ . These unbiased results show that the double occupancy fails to capture the metal-insulator crossover physics. Similar results were recently obtained for the triangular lattice Hubbard model with dynamical cluster approximation [35]. We have also calculated other physical quantities including the compressibility, fidelity susceptibility and Matsubara-frequency self-energy, and also find that they share similar behavior as the double occupancy regarding the crossover [51].

In summary, we have revealed that, in half-filled 3D Hubbard model, a metal-insulator crossover exists between the Fermi liquid and Mott insulator in a considerable range of interaction strength, instead of the conventional Mott transition. This crossover regime is accompanied by strong AFM spin correlations. We find that the metal-insulator crossover can be correctly characterized by the local single-particle spectral function and thermal entropy. The former loses coherence peak at Fermi energy while the latter shows a local maximum when entering the crossover regime. The results of entropy versus interaction also show interesting behaviors regarding the spin and charge fluctuations. The end of the crossover as onset of the Mott insulator is determined from the quasi-particle weight and the appearance of gap in spectra. We have also found that some commonly used observables are not able to characterize the metal-insulator crossover in the model, especially the double occupancy. Our work belongs to one of the only few unbiased studies for the crossover physics, and can also provide timely and important guidance for the optical lattice experiment that has been most recently realized at a nearly uniform optical lattice of large scale [56].

Y.-Y.He acknowledges xxx and xxx for valuable discussions. This work was supported by the National Natural Science Foundation of China (under Grants No. 12047502, No. 12204377, and No. 12275263), the Innovation Program for Quantum Science and Technology (under Grant No. 2021ZD0301900), the Natural Science Foundation of Fujian province of China (under Grant No. 2023J02032), and the Youth Innovation Team of Shaanxi Universities.

\* yjdeng@ustc.edu.cn

† heyuanyao@nwu.edu.cn

- [1] F. Gebhard, *The mott metal-insulator transition: Models and methods* (Springer-Verlag, Berlin Heidelberg, 1997).
- [2] M. Imada, A. Fujimori, and Y. Tokura, Metal-insulator transitions, *Rev. Mod. Phys.* **70**, 1039 (1998).
- [3] F. J. Morin, Oxides which show a metal-to-insulator transition at the neel temperature, *Phys. Rev. Lett.* **3**, 34 (1959).
- [4] S. A. Carter, T. F. Rosenbaum, J. M. Honig, and J. Spalek, New phase boundary in highly correlated, barely metallic  $v_2o_3$ , *Phys. Rev. Lett.* **67**, 3440 (1991); S. A. Carter, T. F. Rosenbaum, P. Metcalf, J. M. Honig, and J. Spalek, Mass enhancement and magnetic order at the mott-hubbard transition, *Phys. Rev. B* **48**, 16841 (1993).
- [5] J. G. Ramirez, T. Saerbeck, S. Wang, J. Trastoy, M. Malnou, J. Lesueur, J.-P. Crocombette, J. E. Villegas, and I. K. Schuller, Effect of disorder on the metal-insulator transition of vanadium oxides: Local versus global effects, *Phys. Rev. B* **91**, 205123 (2015).
- [6] Z. Yang, C. Ko, and S. Ramanathan, Oxide electronics utilizing ultrafast metal-insulator transitions, *Annual Review of Materials Research* **41**, 337 (2011).
- [7] Y. Cao, V. Fatemi, A. Demir, S. Fang, S. L. Tomarken, J. Y. Luo, J. D. Sanchez-Yamagishi, K. Watanabe, T. Taniguchi, E. Kaxiras, R. C. Ashoori, and P. Jarillo-Herrero, Correlated insulator behaviour at half-filling in magic-angle graphene superlattices, *Nature* **556**, 80 (2018).
- [8] Y. Xu, S. Liu, D. A. Rhodes, K. Watanabe, T. Taniguchi, J. Hone, V. Elser, K. F. Mak, and J. Shan, Correlated insulating states at fractional fillings of moiré superlattices, *Nature* **587**, 214 (2020).
- [9] H. Li, S. Li, E. C. Regan, D. Wang, W. Zhao, S. Kahn, K. Yumigeta, M. Blei, T. Taniguchi, K. Watanabe, S. Tongay, A. Zettl, M. F. Crommie, and F. Wang, Imaging two-dimensional generalized wigner crystals, *Nature* **597**, 650 (2021).
- [10] A. Georges, G. Kotliar, W. Krauth, and M. J. Rozenberg, Dynamical mean-field theory of strongly correlated fermion systems and the limit of infinite dimensions, *Rev. Mod. Phys.* **68**, 13 (1996).
- [11] P. Limelette, P. Wzietek, S. Florens, A. Georges, T. A. Costi, C. Pasquier, D. Jérôme, C. Mézière, and P. Batail, Mott transition and transport crossovers in the organic compound  $\kappa$ -(BEDT-TTF) $_2$ Cu[N(CN) $_2$ ]Cl, *Phys. Rev. Lett.* **91**, 016401 (2003).
- [12] A. Ghiotto, E.-M. Shih, G. S. S. G. Pereira, D. A. Rhodes, B. Kim, J. Zang, A. J. Millis, K. Watanabe, T. Taniguchi, J. C. Hone, L. Wang, C. R. Dean, and A. N. Pasupathy, Quantum criticality in twisted transition metal dichalcogenides, *Nature* **597**, 345 (2021).
- [13] T. Li, S. Jiang, L. Li, Y. Zhang, K. Kang, J. Zhu, K. Watanabe, T. Taniguchi, D. Chowdhury, L. Fu, J. Shan, and K. F. Mak, Continuous mott transition in semiconductor moiré superlattices, *Nature* **597**, 350 (2021).
- [14] S. Kim, T. Senthil, and D. Chowdhury, Continuous mott transition in moiré semiconductors: Role of long-wavelength inhomogeneities, *Phys. Rev. Lett.* **130**,

- 066301 (2023).
- [15] N. F. Mott, The basis of the electron theory of metals, with special reference to the transition metals, *Proceedings of the Physical Society. Section A* **62**, 416 (1949).
- [16] N. F. Mott, Metal-insulator transition, *Rev. Mod. Phys.* **40**, 677 (1968).
- [17] J. Hubbard, Electron correlations in narrow energy bands, *Proc. R. Soc. Lond. A* **276**, 238 (1963).
- [18] F. J. Ohkawa, Mott metal-insulator transition in the hubbard model, arXiv: [0707.0142](https://arxiv.org/abs/0707.0142) (2007).
- [19] J. M. Kurdestany and S. Satpathy, Mott metal-insulator transition in the doped hubbard-holstein model, *Phys. Rev. B* **96**, 085132 (2017).
- [20] H. Pan and S. Das Sarma, Interaction-driven filling-induced metal-insulator transitions in 2d moiré lattices, *Phys. Rev. Lett.* **127**, 096802 (2021).
- [21] A. Georges and G. Kotliar, Hubbard model in infinite dimensions, *Phys. Rev. B* **45**, 6479 (1992); A. Georges and W. Krauth, Numerical solution of the  $d=\infty$  hubbard model: Evidence for a mott transition, *Phys. Rev. Lett.* **69**, 1240 (1992); Physical properties of the half-filled hubbard model in infinite dimensions, *Phys. Rev. B* **48**, 7167 (1993).
- [22] M. J. Rozenberg, X. Y. Zhang, and G. Kotliar, Mott-hubbard transition in infinite dimensions, *Phys. Rev. Lett.* **69**, 1236 (1992).
- [23] X. Y. Zhang, M. J. Rozenberg, and G. Kotliar, Mott transition in the  $d=\infty$  hubbard model at zero temperature, *Phys. Rev. Lett.* **70**, 1666 (1993).
- [24] M. J. Rozenberg, R. Chitra, and G. Kotliar, Finite temperature mott transition in the hubbard model in infinite dimensions, *Phys. Rev. Lett.* **83**, 3498 (1999).
- [25] A. Liebsch, Mott transitions in multiorbital systems, *Phys. Rev. Lett.* **91**, 226401 (2003).
- [26] O. Parcollet, G. Biroli, and G. Kotliar, Cluster dynamical mean field analysis of the mott transition, *Phys. Rev. Lett.* **92**, 226402 (2004).
- [27] R. Arita and K. Held, Orbital-selective mott-hubbard transition in the two-band hubbard model, *Phys. Rev. B* **72**, 201102 (2005).
- [28] S. Hoshino and P. Werner, Spontaneous orbital-selective mott transitions and the jahn-teller metal of  $A_3C_{60}$ , *Phys. Rev. Lett.* **118**, 177002 (2017).
- [29] S. Moukouri and M. Jarrell, Absence of a slater transition in the two-dimensional hubbard model, *Phys. Rev. Lett.* **87**, 167010 (2001).
- [30] S. Onoda and M. Imada, Mott transitions in the two-dimensional half-filled hubbard model: Correlator projection method with projective dynamical mean-field approximation, *Phys. Rev. B* **67**, 161102 (2003).
- [31] Y. Z. Zhang and M. Imada, Pseudogap and mott transition studied by cellular dynamical mean-field theory, *Phys. Rev. B* **76**, 045108 (2007).
- [32] H. Park, K. Haule, and G. Kotliar, Cluster dynamical mean field theory of the mott transition, *Phys. Rev. Lett.* **101**, 186403 (2008).
- [33] M. Kohno, Mott transition in the two-dimensional hubbard model, *Phys. Rev. Lett.* **108**, 076401 (2012).
- [34] C. Walsh, P. Sémon, D. Poulin, G. Sordi, and A.-M. S. Tremblay, Thermodynamic and information-theoretic description of the mott transition in the two-dimensional hubbard model, *Phys. Rev. B* **99**, 075122 (2019).
- [35] P.-O. Downey, O. Gingras, J. Fournier, C.-D. Hébert, M. Charlebois, and A.-M. S. Tremblay, Mott transition, widom line, and pseudogap in the half-filled triangular lattice hubbard model, *Phys. Rev. B* **107**, 125159 (2023).
- [36] F. Šimkovic, J. P. F. LeBlanc, A. J. Kim, Y. Deng, N. V. Prokof'ev, B. V. Svistunov, and E. Kozik, Extended crossover from a fermi liquid to a quasiantiferromagnet in the half-filled 2d hubbard model, *Phys. Rev. Lett.* **124**, 017003 (2020).
- [37] A. J. Kim, F. Simkovic, and E. Kozik, Spin and charge correlations across the metal-to-insulator crossover in the half-filled 2d hubbard model, *Phys. Rev. Lett.* **124**, 117602 (2020).
- [38] R. T. Scalettar, D. J. Scalapino, R. L. Sugar, and D. Toussaint, Phase diagram of the half-filled 3d hubbard model, *Phys. Rev. B* **39**, 4711 (1989).
- [39] R. Staudt, M. Dzierzawa, and A. Muramatsu, Phase diagram of the three-dimensional hubbard model at half filling, *The European Physical Journal B* **17**, 411 (2000).
- [40] F. Werner, O. Parcollet, A. Georges, and S. R. Hassan, Interaction-induced adiabatic cooling and antiferromagnetism of cold fermions in optical lattices, *Phys. Rev. Lett.* **95**, 056401 (2005).
- [41] S. Iskakov and E. Gull, Phase transitions in partial summation methods: Results from the three-dimensional hubbard model, *Phys. Rev. B* **105**, 045109 (2022).
- [42] C. Lenihan, A. J. Kim, F. Šimkovic, and E. Kozik, Evaluating second-order phase transitions with diagrammatic monte carlo: Néel transition in the doped three-dimensional hubbard model, *Phys. Rev. Lett.* **129**, 107202 (2022).
- [43] R. R. DeMarco, E. N. Economou, and C. T. White, Random one-body approximation to the hubbard model. iii. application to higher-dimensional lattices, *Phys. Rev. B* **18**, 3968 (1978).
- [44] M. Campostrini, M. Hasenbusch, A. Pelissetto, P. Rossi, and E. Vicari, Critical exponents and equation of state of the three-dimensional heisenberg universality class, *Phys. Rev. B* **65**, 144520 (2002).
- [45] R. Blankenbecler, D. J. Scalapino, and R. L. Sugar, Monte carlo calculations of coupled boson-fermion systems. i, *Phys. Rev. D* **24**, 2278 (1981).
- [46] J. E. Hirsch, Discrete hubbard-stratonovich transformation for fermion lattice models, *Phys. Rev. B* **28**, 4059 (1983).
- [47] S. R. White, D. J. Scalapino, R. L. Sugar, E. Y. Loh, J. E. Gubernatis, and R. T. Scalettar, Numerical study of the two-dimensional hubbard model, *Phys. Rev. B* **40**, 506 (1989).
- [48] R. T. Scalettar, R. M. Noack, and R. R. P. Singh, Ergodicity at large couplings with the determinant monte carlo algorithm, *Phys. Rev. B* **44**, 10502 (1991).
- [49] T. McDaniel, E. F. D'Azevedo, Y. W. Li, K. Wong, and P. R. C. Kent, Delayed Slater determinant update algorithms for high efficiency quantum Monte Carlo, *The Journal of Chemical Physics* **147**, 174107 (2017).
- [50] Y.-Y. He, M. Qin, H. Shi, Z.-Y. Lu, and S. Zhang, Finite-temperature auxiliary-field quantum monte carlo: Self-consistent constraint and systematic approach to low temperatures, *Phys. Rev. B* **99**, 045108 (2019).
- [51] Y.-F. Song, Y. Deng, and Y.-Y. He, Finite-temperature auxiliary-field quantum monte carlo study of the three-dimensional hubbard model, appear soon.
- [52] J. Vučićević, D. Tanasković, M. J. Rozenberg, and V. Dobrosavljević, Bad-metal behavior reveals mott quantum criticality in doped hubbard models, *Phys. Rev. Lett.*

- [114](#), [246402](#) (2015).
- [53] A. W. Sandvik, Constrained sampling method for analytic continuation, *Phys. Rev. E* **94**, 063308 (2016).
- [54] H. Shao and A. W. Sandvik, Progress on stochastic analytic continuation of quantum monte carlo data, *Physics Reports* **1003**, 1 (2023), progress on stochastic analytic continuation of quantum Monte Carlo data.
- [55] Z. Zhu, D. N. Sheng, and L. Fu, Spin-orbital density wave and a mott insulator in a two-orbital hubbard model on a honeycomb lattice, *Phys. Rev. Lett.* **123**, 087602 (2019).
- [56] H.-J. Shao, Y.-X. Wang, D.-Z. Zhu, Y.-S. Zhu, H.-N. Sun, S.-Y. Chen, C. Zhang, Z.-J. Fan, Y. Deng, X.-C. Yao, Y.-A. Chen, and J.-W. Pan, Observation of the antiferromagnetic phase transition in the fermionic hubbard model, *arXiv*: [2402.14605](#) (2024).